S100A1 and Calmodulin Compete for the Same Binding Site on Ryanodine Receptor*

Nathan T. Wright[‡1,2], **Benjamin L. Prosser**[‡1], **Kristen M. Varney**[‡], **Danna B. Zimmer**[§], **Martin F. Schneider**[‡], **and David J. Weber**[‡3]

From the ‡Department of Biochemistry and Molecular Biology, University of Maryland School of Medicine, Baltimore, Maryland 21201 and the §Department of Veterinary Pathobiology, College of Veterinary Medicine, Texas A&M University, College Station, Texas 77843-44467

In heart and skeletal muscle an S100 protein family member, S100A1, binds to the ryanodine receptor (RyR) and promotes Ca^{2+} release. Using competition binding assays, we further characterized this system in skeletal muscle and showed that Ca^{2+}-S100A1 competes with Ca^{2+}-calmodulin (CaM) for the same binding site on RyR1. In addition, the NMR structure was determined for Ca^{2+}-S100A1 bound to a peptide derived from this CaM/S100A1 binding domain, a region conserved in RyR1 and RyR2 and termed RyRP12 (residues 3616–3627 in human RyR1). Examination of the S100A1-RyRP12 complex revealed residues of the helical RyRP12 peptide (Lys-3616, Trp-3620, Lys-3622, Leu-3623, Leu-3624, and Lys-3626) that are involved in favorable hydrophobic and electrostatic interactions with Ca^{2+}-S100A1. These same residues were shown previously to be important for RyR1 binding to Ca^{2+}-CaM. A model for regulating muscle contraction is presented in which Ca^{2+}-S100A1 and Ca^{2+}-CaM compete directly for the same binding site on the ryanodine receptor.

Excitation coupling is a process by which sarcolemmal depolarization triggers Ca^{2+} release from the sarcoplasmic reticulum (SR),[4] leading to Ca^{2+} activation of the thin filaments and muscle fiber contraction. The ryanodine receptor (RyR1) is the primary SR Ca^{2+} release channel in skeletal muscle and is mechanically coupled to the dihydropyridine receptor (Ca_V 1.1 L-type channel) (reviewed in Ref. 1). A second isoform, RyR2, regulates calcium release in cardiac muscle in response to a cytosolic Ca^{2+} influx generated from another dihydropyridine receptor L-type channel (Ca_V 1.2 L-type channel). For both cardiac and skeletal muscle, RyR-dependent calcium release is modulated by ions such as Ca^{2+} and Mg^{2+}, as well as by several small soluble proteins, including FKBP12 and CaM (2–4). Recently, several studies demonstrated that an S100 protein, S100A1, enhances RyR1- and RyR2-dependent calcium release in both skeletal and cardiac muscle, respectively (5–10). Specifically, S100A1 knock-out skeletal muscle fibers demonstrate decreased Ca^{2+} transients (6), and adenoviral delivery of S100A1 into failing cardiomyocytes restores myocyte contractile properties (11). Additionally, S100A1 increases [³H]ryanodine binding to RyR1, indicative of increased activation of the channel (5), and S100A1 binds directly to RyR1 in a calcium-dependent manner (6). These data suggest a possible therapeutic role of S100A1 in treatment strategies for skeletal and cardiomyopathies (6, 8, 11).

S100A1 is a symmetric homodimer (93 residues/subunit) with each S100A1 subunit having a low affinity pseudo-EF hand and a second high affinity canonical EF hand calcium binding domain (12). The solution structures of apo- and Ca^{2+}-S100A1 were solved previously using NMR methods (12, 13), and show that a large reorientation of helix 3 occurs in S100A1 upon the addition of calcium. This conformational change exposes a hydrophobic pocket on each S100A1 subunit (12, 14), providing a binding site for target proteins such as RyR1 and RyR2. Here we show that a 12-residue peptide (termed RyRP12), derived from the CaM/S100A1-binding site on both RyR1 and RyR2, interacts with a major portion of the target protein-binding site on Ca^{2+}-S100A1 (6, 15, 16). We present the solution NMR structure of RyRP12 bound to Ca^{2+}-S100A1, which has several striking similarities to that observed previously for the RyR1 (residues 3614–3643 in human)-CaM complex (17). Furthermore, competition binding experiments show that Ca^{2+}-S100A1 competes directly with an RyR antagonist, Ca^{2+}-CaM, for the same binding site on RyR1 and could explain how S100A1 promotes Ca^{2+} release in skeletal and heart muscle.

EXPERIMENTAL PROCEDURES

Fluo-4 AM Fluorescent Recordings—FDB fibers were isolated from transgenic S100A1 KO mice and their wild type age-matched, sex-matched littermates (described in Ref. 6). Follow-

ing enzymatic dissociation and ~24 h in culture, FDB skeletal fiber cultures were loaded with 2 μM Fluo-4 AM in 0.1% DMSO for 30 min, rinsed with Ringer's solution three times, and equilibrated for 30 min before recording. The culture chamber was then mounted on an Olympus IX-70 inverted microscope using a $60\times/1.20$ NA water immersion objective coupled to a cell map laser scanning confocal system (Bio-Rad). The system was operated in line scan x-t mode at a scanning speed of 2 ms/line for 512 ms. Line scan images were processed, and fluorescent recordings were converted to $\Delta F/F_0$ values. Statistical analysis was performed using OriginPro 7.5. All significance tests were done using Student's t test, and significance was set at $p < 0.05$.

Western Blots—Recombinant S100A1 was attached to CH-Sepharose beads (Sigma) using standard methods. Intact RyR in SR vesicles were prepared as described previously and bound to S100A1 beads in the presence of calcium (100 nM to 1.0 mM) prior to competition experiments with variable concentrations of calmodulin (6). After incubation, 8-μl aliquots of the S100A1-linked beads were washed, boiled, and loaded into an SDS-polyacrylamide gel. An anti-RyR antibody (C34)(Sigma) was used to detect RyR, and ImageJ software, available on the National Institutes of Health website, was used to quantify the intensity of each band from the Western blot.

Sample Preparations—A synthetic peptide derived from the S100A1/calmodulin binding domain of human RyR1 (residues 3616–3627) was chemically synthesized and prepared for NMR as described previously (6). Recombinant ^{15}N- and ^{13}C,^{15}N-labeled S100A1 human S100A1 protein was purified after over-expression in *Escherichia coli* (HMS174(DE3)) as described (12). NMR samples contained 15 mM d_{11}-Tris-HCl, pH 7.2, 15 mM dithiothreitol, 10 mM CaCl₂, 0.34 mM NaN₃, 20 mM NaCl, 10% ^{2}H₂O, RyRP12 peptide (2–6 mM), and S100A1 (1–3 mM; subunit concentration). Acrylamide solutions used for dipolar coupling experiments were prepared as described previously (12).

NMR Spectroscopy and Chemical Shift Assignments—NMR spectra were collected at 37 °C with a Bruker DMX600 NMR spectrometer (600.13 MHz for protons) and a Bruker AVANCE 800 NMR spectrometer (800.27 MHz for protons), each equipped with four frequency channels and 5-mm triple-resonance z-axis gradient cryogenic probe heads. Sequential backbone and side chain assignments of S100A1 in the RyRP12 peptide complex were obtained using standard NMR spectroscopy methods as described (6, 12). The sequential assignments for the unlabeled RyRP12 peptide bound to ^{13}C,^{15}N-labeled Ca²⁺-S100A1 were based on correlations recorded in ^{15}N- and ^{13}C-filtered TOCSY and ^{15}N- and ^{13}C-filtered NOESY experiments (31, 32). The filtered TOCSY spinlock time was 75 ms, and the filtered NOESY mixing time was 200 ms. The backbone and side chain ^{1}H, ^{13}C, and ^{15}N chemical shift assignments are complete. Chemical shifts assignments for S100A1 and the RyRP12 peptide in the RyRP12-Ca²⁺-S100A1 complex have been deposited in the BioMagResBank (accession numbers 15296 and 15704).

Structure Calculations—Interproton distance constraints were derived from two-, three-, and four-dimensional NOESY experiments (two-dimensional NOESY, ^{12}C-filtered two-di-
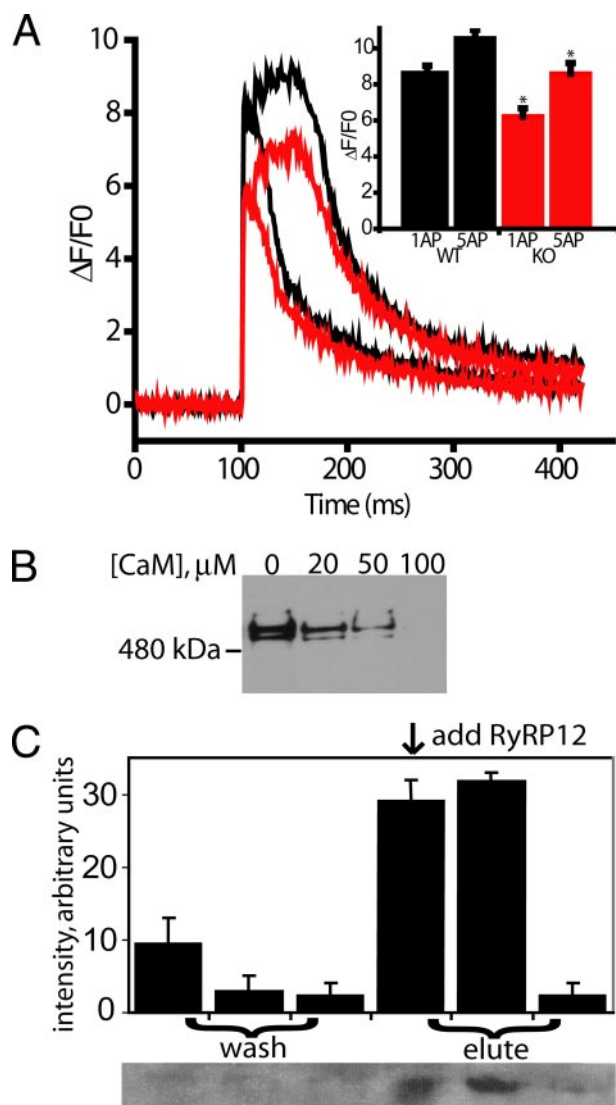
FIGURE 1. **S100A1 binding and enhancement of RyR1 function in skeletal muscle.** *A*, S100A1$^{-/-}$ muscle fibers (*red*) demonstrate decreased amplitude of Ca²⁺ transients following single (*1AP*) and multiple (*5AP*, 100 Hz) action potential stimulation compared with WT age- and sex-matched littermates (*black*). Fluo-4 AM-loaded adult FDB muscle fibers from WT and S100A1 KO mice were stimulated with field electrodes and assayed for Ca²⁺ transient responses using confocal line scan microscopy. KO fibers showed significantly decreased peak amplitude of Ca²⁺ transients following 1AP (WT = 8.62 ± 0.41; *n* = 6, KO = 6.22 ± 0.45; *n* = 6, *, *p* = 0.003) and 5AP stimulation (WT = 10.54 ± 0.49; *n* = 6, KO = 8.59 ± 0.59; *n* = 6, *, *p* = 0.036), when compared with WT controls. *B*, at 5 μM Ca²⁺ concentration, calmodulin competes with S100A1-linked Sepharose beads bound to intact RyR1 in a concentration-dependent manner. The RyR does not bind to S100A1-linked Sepharose beads in the absence of calcium (data not shown). *C*, full-length RyR is eluted from S100A1-linked Sepharose beads upon addition of 3 μM RyRP12 peptide in 1 mM Ca²⁺.

mensional NOESY, ^{15}N-edited three-dimensional NOESY, ^{12}C-filtered and ^{13}C-edited three-dimensional NOESY, ^{15}N- and ^{13}C-edited four-dimensional NOESY, and ^{13}C and ^{13}C-edited four-dimensional NOESY) as described previously (6, 12). Dihedral constraints $\phi \pm 20$ and $\psi \pm 15°$ for α-helix and $\phi \pm 40$ and $\psi \pm 40°$ for β-sheet were included based on $^3J_{NH-H\alpha}$ coupling constants, hydrogen exchange rates, and the chemical shift index (35) of ^{1}Hα and ^{13}Cα atoms. Distance constraints of 2.0–2.8 Å between Ca²⁺ and protein ligands were included based on the EF-hand model for a typical and S100-type cal-
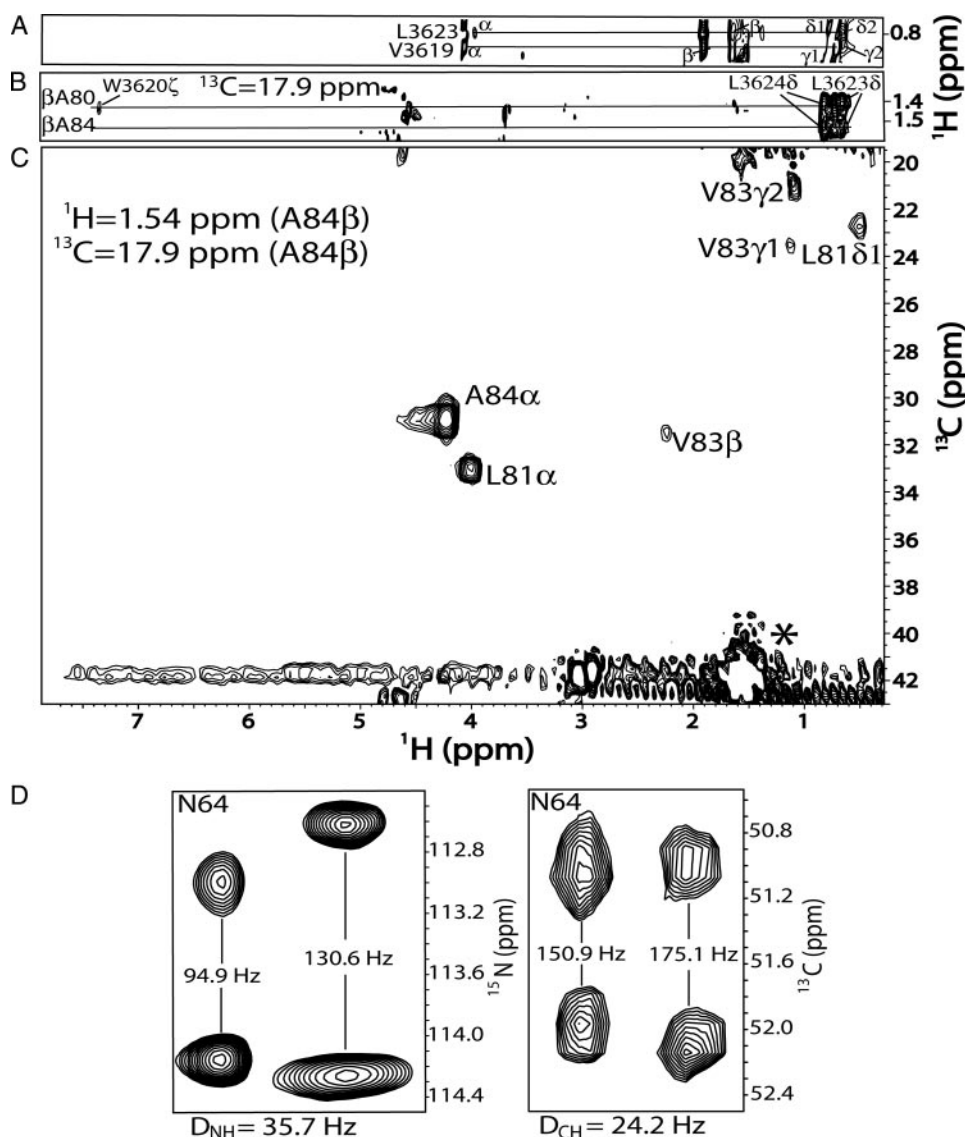
FIGURE 2. **NMR data from the RyRP12-Ca²⁺-S100A1 complex.** *A,* strip from the two-dimensional ¹²C-filtered TOCSY illustrating proton assignments of Leu-3623 and Val-3619 of the RyRP12 peptide when bound to Ca²⁺-S100A1. *B,* strip from a plane of the three-dimensional ¹³C-edited, ¹²C-filtered NOESY experiment illustrating intermolecular NOE correlations between Ala-80 and Ala-84 of Ca²⁺-S100A1 with several residues from the RyRP12 peptide. *C,* a plane from the four-dimensional ¹³C, ¹³C-edited NOESY spectrum illustrating S100A1 NOE correlations to Ala-β84 in the RyRP12-Ca²⁺-S100A1 complex. The contour labeled with an *asterisk* is the auto-correlation peak and unlabeled NOE correlations maximize in different planes. *D,* residual dipolar coupling data illustrating typical N-H^N and Cᵅ-Hᵅ splittings for Asn-64 of S100A1 in the RyRP12-Ca²⁺-S100A1 complex in isotropic (*left*) and aligned (*right*) media.

out Hᵅ decoupling during Cᵅ acquisition in t_2 to record Cᵅ-Hᵅ splittings, as described previously (12, 37, 38). These residual dipolar couplings were incorporated into the final structure calculation as described previously (12). The final 20 structures were selected (from 200) based on lowest energy and were of high quality based on the statistical criteria listed in Table 1. The coordinates of the RyRP12-Ca²⁺-S100A1 structure have been deposited in the Protein Data Bank (accession number 2K2F).

RESULTS

S100A1 Binding to the CaM-binding Site on RyR1 Positively Modulates Calcium Release—In both skeletal and heart muscle, S100A1 modulates excitation coupling by promoting calcium release from SR stores (6, 8, 10). In skeletal muscle, S100A1 binds to the cal-modulin binding domain (CaMBD, residues 3614–3643) of RyR1 and activates Ca²⁺ release via the channel during single action potential (5, 6). To further test this model, calcium transients arising from electrically stimulated FDB muscle fibers were compared here in wild type (WT) and S100A1 knock-out (KO) mice (Fig. 1*A*). Calcium transients arising from single and repetitive action potential (AP) stimulation were both diminished by ~25% in S100A1 knockouts *versus* WT fibers (Fig. 1*A*). These data are consistent with previous studies that showed S100A1 positively modulates SR Ca²⁺ release and corresponding fractional myocyte shortening (5, 6, 8, 10).

It is now generally recognized that exogenous CaM regulates calcium release from the SR by binding most tightly to a single conserved site on RyR1 and RyR2 (15–18). S100A1 binds this same high affinity site on RyR1 (6); however, the question remained whether S100A1 binds tightly to just this single region or whether multiple high affinity S100A1-binding sites exist on the intact RyR channel (5, 6). To address this issue directly, SR vesicles containing intact RyR1 were incubated with Sepharose-linked S100A1 beads at high [Ca²⁺] in the presence of increasing amounts of CaM. As observed in Fig. 1*B*, CaM fully displaced RyR1 from the S100A1 beads in a concentration-dependent manner indicating that S100A1 binds to the same region as CaM in the intact RyR. Because

cium binding domain, respectively (33). The inclusion of such restraints had no effect on the overall structure of the complex. Hydrogen bond constraints of $r_{HN-O} = 1.5–2.8$ Å and $r_{N-O} = 2.4–2.5$ Å were included in the final stage of structure calculations. Pseudopotentials for secondary ¹³Cᵅ and ¹³Cᵝ chemical shifts and a conformational data base potential were included in the final simulated annealing refinements using the computer program XPLOR (36). The internuclear dipolar couplings (in Hz) were determined from the difference in *J* splitting between isotropic and axially compressed polyacrylamide-aligned phases, using both a two-dimensional IPAP ¹H-¹⁵N heteronuclear single quantum coherence to record N-H^N splittings and a three-dimensional CT-(H)CA(CO)NH experiment with-
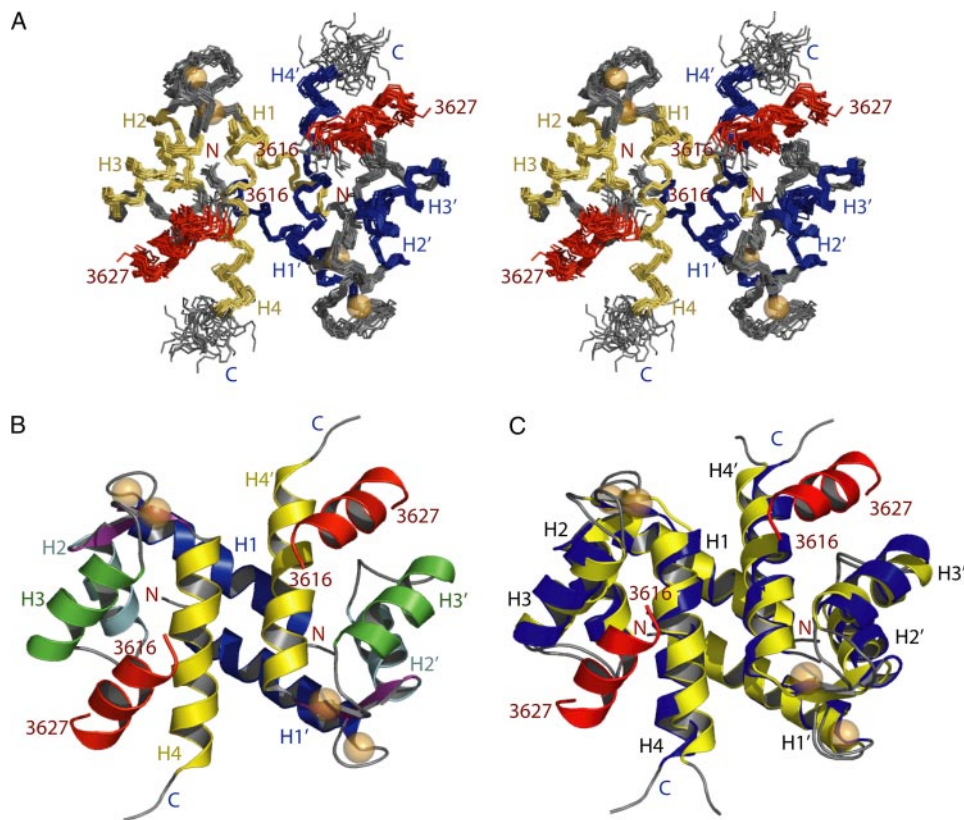
FIGURE 3. **The three-dimensional structure of the Ca²⁺-S100A1-RyRP12 complex.** *A,* stereoview of the 20 lowest energy structures. The r.m.s.d. of the entire complex, (3–87 A1 and 2–11 RyRP12) is 0.68 for the backbone atoms. The S100A1 subunits 1 and 2 are colored *tan* and *blue,* respectively, and the RyRP12 peptide is colored *red. B,* ribbon diagram of the Ca²⁺-S100A1-RyRP12 complex. *C,* overlay of the Ca²⁺-S100A1 complex (*yellow*) with the Ca²⁺-S100A1-RyRP12 complex (*blue*) illustrating small conformational changes in Ca²⁺-S100A1 upon the addition or RyRP12. The r.m.s.d. of C$^\alpha$ atoms between the two structures (residues 3–88) is 1.60 Å.

ments and are described in Prosser *et al.* (6). Unambiguous resonance and NOE assignments for the unlabeled RyRP12 peptide bound to ¹³C-, ¹⁵N-labeled S100A1 were made using two-dimensional ¹²C-filtered spectra (NOESY, TOCSY in H$_2$O and D$_2$O), which removed all resonances arising from the labeled S100A1 (Fig. 2*A*). With the same sample in H$_2$O, a three-dimensional ¹³C-edited, ¹²C-filtered NOESY experiment was then collected to assign intermolecular NOE correlations between ¹³C,¹⁵N-labeled S100A1 and unlabeled RyRP12 peptide (Fig. 2*B*). This NMR experiment detects only NOE correlations between protons attached to ¹³C and protons attached to ¹²C; therefore, only those NOE correlations at the peptide (¹²C)–protein (¹³C) interface are detected. Unambiguous assignment of intramolecular NOE correlations for Ca²⁺-S100A1 in the protein-peptide complex was achieved via three-dimensional ¹⁵N-edited NOESY, three-dimensional ¹³C-edited NOESY, four-dimensional ¹⁵N- and ¹³C-edited NOESY, and four-dimensional ¹³C

residues 3416–3427 of the CaMBD very closely resemble the canonical S100-binding sequence (RyRP12: Lys-Lys-Ala-Val-Trp-His-Lys-Leu-Leu-Ser-Lys-Gln; underlined residues are the S100 consensus binding sequence), we next tested whether RyRP12 could compete with full-length RyR1 binding to Sepharose-S100A1 beads in the presence of micromolar [Ca²⁺]. Fig. 1*C* shows that RyRP12 was sufficient to elute intact full-length RyR1 from Sepharose-S100A1 beads, providing evidence that this peptide includes a major portion of the S100A1-binding site on RyR1.

Taken together, these results show that S100A1 competes with CaM for the same binding site of RyR1 and that the RyRP12 peptide can disrupt a complex involving S100A1 and full-length RyR1. Furthermore, genetic deletion of S100A1 significantly decreased calcium release from the SR of skeletal muscle. Given that the RyRP12-S100A1 complex is both structurally and functionally relevant in modulating SR calcium release in skeletal muscle, we solved the solution structure of RyRP12 bound to Ca²⁺-S100A1.

Solution NMR Structure of Ca²⁺-S100A1 Bound to RyRP12— The size of the RyRP12-S100A1 complex (24 kDa) necessitated the collection of a series of heteronuclear multidimensional NMR experiments to determine its structure in solution. The ¹H, ¹³C, and ¹⁵N chemical shift assignments for the backbone and side chain resonances of Ca²⁺-S100A1 bound to RyRP12 were conducted using standard NMR through-bond experi-

and ¹³C-edited NOESY experiments (Fig. 2*C*). In an effort to both improve and independently verify the NOE-based structure (20), both N-H^N and C$^\alpha$-H$^\alpha$ residual dipolar coupling data were also included in the structure calculations (Fig. 2*D*).

In total, 3,306 experimental distance constraints, 278 dihedral angle constraints, and 116 residual dipolar coupling constraints were used to calculate the solution structure of the Ca²⁺-S100A1-RyRP12 complex (>17 constraints/residue). Importantly, the S100A1-bound RyRP12 peptide has more than 11 constraints/residue on average, which allowed for an accurate residue-by-residue examination of the S100A1-RyRP12 binding interface. A family of the 20 best Ca²⁺-S100A1-RyRP12 structures is depicted in stereoview in Fig. 3*A*. These structures all have low *Q*-factors; no dihedral violations greater than 5°, no NOE violations greater than 0.4 Å, and no residues in the unfavorable portion of the Ramachandran plot (Table 1). The backbone atoms in each of the 20 S100A1 subunits are well defined with an r.m.s.d. of 0.57 for all ordered residues. For the bound RyRP12 peptide, the backbone is slightly less well defined, with an r.m.s.d. of 0.95 for all ordered residues (Table 1). No long range NOE correlations were observed for residues 1–2 and 88–93 in Ca²⁺-S100A1 or for residues 1 and 12 in RyRP12, so these residues were not included in the r.m.s.d. calculation.

Upon binding calcium, helix 3 of S100A1 undergoes a large reorientation from being nearly antiparallel to being

TABLE 1

NMR-derived restraints and statistics of 20 NMR structures

The 20 ensemble structures, ⟨20⟩, are the results of simulated annealing calculations. The best structure is the closest to the average structure. The values shown for the ⟨20⟩ are the mean ± S.D.

	⟨20⟩	Best
r.m.s.d. from distance constraints (Å)[a]		
Total (3306)	0.034 ± 0.001	0.035
Intraresidue (574)	0.004 ± 0.003	0.003
Sequential ($|i - j| = 1$) (934)	0.032 ± 0.003	0.033
Medium range ($1 < |i - j| \leq 1$) (830)	0.035 ± 0.004	0.039
Long range ($|i - j| > 5$) (380)	0.043 ± 0.007	0.034
Intermolecular for dimer interface (102)	0.030 ± 0.010	0.028
Intra- and/or intermolecular (24)	0.004 ± 0.002	0.000
RyRP12 peptide (intrasequential, sequential, medium) (194)	0.034 ± 0.002	0.028
Intermolecular S100A1 to RyRP12 peptide (78)	0.047 ± 0.011	0.034
Calcium ligand (18)	0.024 ± 0.017	0.053
Hydrogen bonds (170)	0.063 ± 0.006	0.069
r.m.s.d. from experimental dihedral constraints (°)		
Φ,Ψ (278)	0.573 ± 0.152	0.563
r.m.s.d. from dipolar coupling restraints (Hz)		
D_{NH} (57)	0.981 ± 0.065	1.090
D_{CH} (59)	1.386 ± 0.140	1.560
r.m.s.d. from experimental ^{13}C chemical shifts		
^{13}C$^\alpha$ (ppm)	1.203 ± 0.052	1.210
^{13}C$^\beta$ (ppm)	1.061 ± 0.045	1.041
r.m.s.d. from idealized geometry		
Bonds (Å)	0.005 ± 0.001	0.005
Angles (°)	0.885 ± 0.017	0.891
Impropers (°)	1.825 ± 0.013	1.827
Lennard-Jones potential energy (kcal/mol)[b]	−852 ± 36	−838
Q-Factor[c]	0.22 ± 0.02	0.18
% of residues in the most favorable region of the Ramachandran plot[d]	88.0 ± 2.1	89.7
r.m.s.d. to the mean structure (Å)[e]		
All backbone atoms in S100A1 (3–87)	0.565 ± 0.103	0.530
All heavy atoms in S100A1 (3–87)	1.107 ± 0.254	1.150
All backbone atoms in RyRP12 peptide (2–11)	0.949 ± 0.302	0.460
All heavy atoms in RyRP12 peptide (2–11)	1.322 ± 0.350	0.974

[a] None of the 20 structures has a distance violation >0.4 Å or a dihedral angle violation of >5°. The force constants used in the SA calculations are as follows: 1000 kcal mol^{-1} Å^2 for bond length, 500 kcal mol^{-1} rad^{-2} for angles and improper torsions, 4 kcal mol^{-1} Å^{-4} for the quartic van der Waals repulsion term (hard-sphere effective van der Waals set to 0.8 times their values in CHARMm parameters), 50 kcal mol^{-1} Å^{-2} for experimental distance constraints, 100 kcal mol^{-1} Å^{-2} for noncrystallographic symmetry, 1 kcal mol^{-1} Å^{-2} for distance symmetry constraints, 0.5 kcal mol^{-1} ppm^{-2} for the ^{13}C chemical shift constraints, and 1.0 for the conformational data base potential. The force constants used for (in kcal Hz^{-2}) used for dipolar coupling restraints were as follows: 0.63 for ^{15}N-^{1}H^N and 0.25 for ^{13}C$^\alpha$-^{1}H$^\alpha$.

[b] Lennard-Jones van der Waals energies were calculated using CHARMm parameters and were not used in any stage of the structure determination.

[c] Q-Factors were determined by randomly removing 10% of all RDC values. To ensure accuracy, an ensemble of structures with a second randomly removed subset of RDCs was also run. The Q-factor of this second set was 0.21.

[d] PROCHECK was utilized to generate the Ramachandran plot.

[e] Backbone calculations include C$^\alpha$, N, and C′ atoms. Only residues 3–87 are included since no long range NOE correlations were observed for residues 1–3 and 87–93 in S100A1 or residues 1 and 12 in the RyRP12 peptide.

TABLE 2

Interhelical angles and distance of various states of S100A1 and S100B

Interhelical angles and interhelical distances were calculated using Ihe version 1.4 (S. M. Gangue, MSG Software, Inc.) using the structures indicated.

	Interhelical angle (degree)								Interhelical distance	
	I to II	I to III	I to IV	II to III	II to IV	III to IV	I to I′	IV to IV′	I to I′	IV to IV′
									Å	Å
Ca^{2+}-S100A1-RyRP12	136 ± 2	−94 ± 2	125 ± 2	126 ± 1	−35 ± 2	136 ± 2	−153 ± 2	156 ± 2	12.3 ± 0.3	12.2 ± 0.3
Ca^{2+}-S100A1[a2]	132 ± 1	−102 ± 2	131 ± 2	125 ± 2	−29 ± 1	121 ± 2	−157 ± 3	152 ± 3	12.5 ± 0.2	11.1 ± 0.4
Apo-S100A1[b]	120 ± 3	−45 ± 2	107 ± 2	148 ± 2	−46 ± 1	−150 ± 1	−165 ± 3	176 ± 2	10.2 ± 0.3	9.9 ± 0.3
Ca^{2+}-S100B-TRTK[c]	132 ± 2	−118 ± 2	128 ± 1	109 ± 2	−33 ± 2	108 ± 4	−148 ± 2	146 ± 3	12.4 ± 0.1	9.3 ± 0.3
Ca^{2+}-S100B[d]	137 ± 5	−188 ± 5	128 ± 4	104 ± 3	−35 ± 4	106 ± 4	−155 ± 5	159 ± 5	14.3 ± 0.5	10.6 ± 0.5
Apo-S100B[e]	133 ± 1	−46 ± 1	120 ± 1	149 ± 1	−40 ± 1	−166 ± 1	−153 ± 1	155 ± 1	13.6 ± 0.3	10.3 ± 0.4

[a] Data were taken from NMR structure (PDB entry 1ZFS) of Wright *et al.* (12).

[b] Data were taken NMR structure (PDB entry 1K2H) of Rustandi *et al.* (13).

[c] Data were taken from NMR structure (PDB entry 1MWN) of Inman *et al.* (21).

[d] Data were taken from NMR structure (PDB entry 1QLK) of Drohat *et al.* (33).

[e] Data were taken from NMR structure (PDB entry 1B4C) of Drohat *et al.* (34).

perpendicular to helix 4 (Table 2) (12). This conformational change exposes a large hydrophobic pocket in Ca^{2+}-S100A1, which is important for binding the RyRP12 peptide (Fig. 3*B*). The RyRP12 peptide adopts a helical conformation when bound to Ca^{2+}-S100A1 with the peptide aligned in an anti-parallel orientation to helix 3 of each monomer in the S100A1 dimer. The orientation of RyRP12 on S100A1 is unlike other S100-peptide complexes in which peptides align in parallel with helix 3 (21–24). Peptide binding produces only minor structural changes in Ca^{2+}-S100A1 with the largest difference between the peptide-bound and peptide-free states being a 15° difference in the helix 3–4 angle (Table 2). This closure of helices 3 and 4 in S100A1 is necessary to optimally interact with RyRP12.
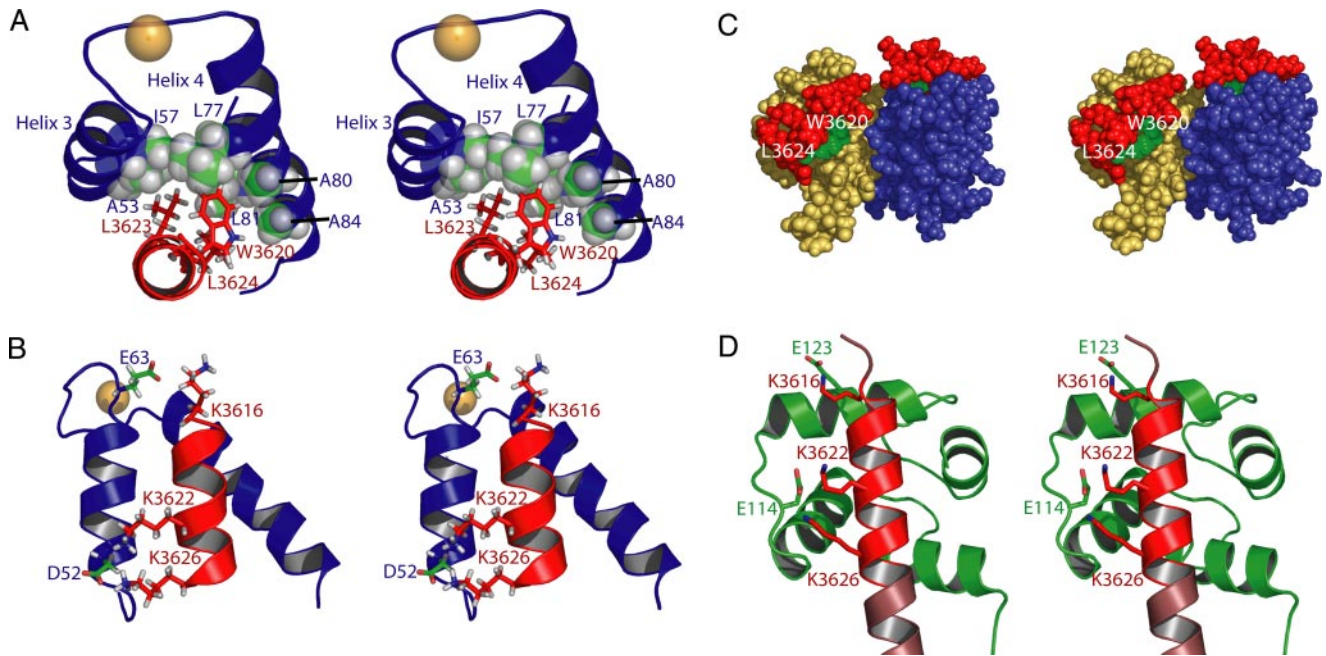
FIGURE 4. **Residues of the RyRP12 peptide (residues 3616 –3627 or RyR1) and S100A1 involved in Ca²⁺-S100A1-RyRP12 complex formation.** *A,* diagram illustrating hydrophobic residues involved in the RyRP12-S100A1 interaction including Ala-53, Ile-57, Leu-77, Ala-80, Leu-81, and Ala-84 of S100A1, and Trp-3620, Leu-3623, and Leu-3624 of RyRP12. *B,* ribbon diagram illustrating hydrophilic residues in the RyRP12-S100A1 complex that are likely involved in ionic interactions, including Asp-52 and Glu-63 on S100A1 and Lys-3616, Lys-3622, and Lys-3627 on the RyRP12 peptide. *C,* space-filling diagram of the S100A1-RyP12 peptide showing residues in *green* (Trp-3620 and Leu-3624) that are important for calmodulin binding to the ryanodine receptor. The rest of the RyRP12 peptide is colored in *red*, and the S100A1 subunits 1 and 2 are colored *tan* and *blue*, respectively. *D,* ribbon diagram of the C-terminal region of CaM bound to the CaMBD of the RyR (residues 3614 –3643 of RyR; Protein Data Bank code 2BCX) (17), showing side chains of the RyR that are involved in ionic interactions with CaM; these same residues are also likely to form salt bridges with negatively charged side chains of Ca²⁺-S100A1.

Bound RyRP12 Peptide and the Binding Interface—In the absence of S100A1, the RyRP12 exists as a random coil, as judged by circular dichroism, a lack of NOE correlations, and a narrow range of dispersion for NMR chemical shift values (data not shown). However, when bound to Ca²⁺-loaded S100A1, most residues in RyRP12 adopt a helical conformation as judged by a significant increase in proton spectral dispersion when compared with free peptide, upfield shifted $^1H^\alpha$ chemical shift values, and by a number of characteristic NOE correlations indicative of helix formation (*i.e.* $\alpha\beta_{i,i+3}$, $\alpha N_{i,i+3}$, etc.). Such a change in a target peptide from a random coil to a helix, as observed here when RyRP12 bound to S100A1, was observed previously for several S100-target peptide interactions (21, 22) and is likely a common occurrence based on the overall similarity in the geometry of the binding pockets for this family of proteins.

The binding surfaces in the Ca²⁺-S100A1-RyRP12 peptide complex are defined by 14 residues from the hinge region (Leu-45 and Asp-46), helix 3 (Asp-52, Ala-53, Lys-56, Ile-57, and Glu-60), and helix 4 (Val-76, Leu-77, Val-78, Ala-80, Leu-81, Ala-84, and Cys-85) on S100A1, which come into contact with six residues (Lys-3616, Trp-3620, Lys-3622, Leu-3623, Leu-3624, and Lys-3627) from RyRP12. Specifically, three hydrophobic residues (Trp-3620, Leu-3623, and Leu-3624) are on the same face of the amphipathic RyRP12 helix and buried in the hydrophobic pocket of S100A1 upon peptide binding (Fig. 4*A*). Additionally, several potential ionic interactions involving Lys-3616, Lys-3622, and Lys-3626 of RyRP12 and Asp-52 and Glu-63 of S100A1 are also likely, based on the NMR structure (Fig. 4*B*). Of interest, all of the charged residues close to the hydrophobic binding pocket on S100A1 are located on one side

of the hydrophobic pocket, at or near the hinge region and helix 3 (Asp-46, Lys-49, Asp-50, Asp-52, Lys-56, Glu-60, and Glu-63), whereas no charged residues from helix 4 contribute to the binding pocket. Thus, the charged residues on helix 3 likely dictate the orientation in which RyRP12 binds to S100A1, and they likely contribute to specificity between S100A1 and its target proteins, including RyR1, because they are not that well conserved in the S100 protein family.

DISCUSSION

As found previously for other S100 proteins (25, 26), S100A1 binds to the RyR in a calcium-dependent manner. The Ca²⁺ dependence of the S100A1-RyRP12 peptide interaction can be understood by comparing the structures of apo-S100A1, Ca²⁺-S100A1, and RyRP12-Ca²⁺-S100A1. Specifically, most of the residues of S100A1 (11 of 14) that are in close contact with the RyRP12 peptide in the S100A1-peptide complex are either partially or fully buried in the apo-form of S100A1 and unavailable for binding RyRP12. However, upon binding calcium, these same residues of S100A1 become solvent-exposed and localized in a single binding pocket because of the large calcium-dependent reorientation of helix 3 (12). Upon binding the RyRP12 peptide, only minor structural changes were observed in the Ca²⁺-S100A1 peptide binding pocket, which are necessary for an optimal protein-peptide interaction (Fig. 3*C*).

The RyRP12 peptide includes part of a well characterized calmodulin-binding site on the ryanodine receptor, and data presented here demonstrate that Ca²⁺-S100A1 and Ca²⁺-CaM compete for this site on RyR1 (Fig. 1*B*). Furthermore, similarities in the mode of binding were observed when the structures of Ca²⁺-S100A1
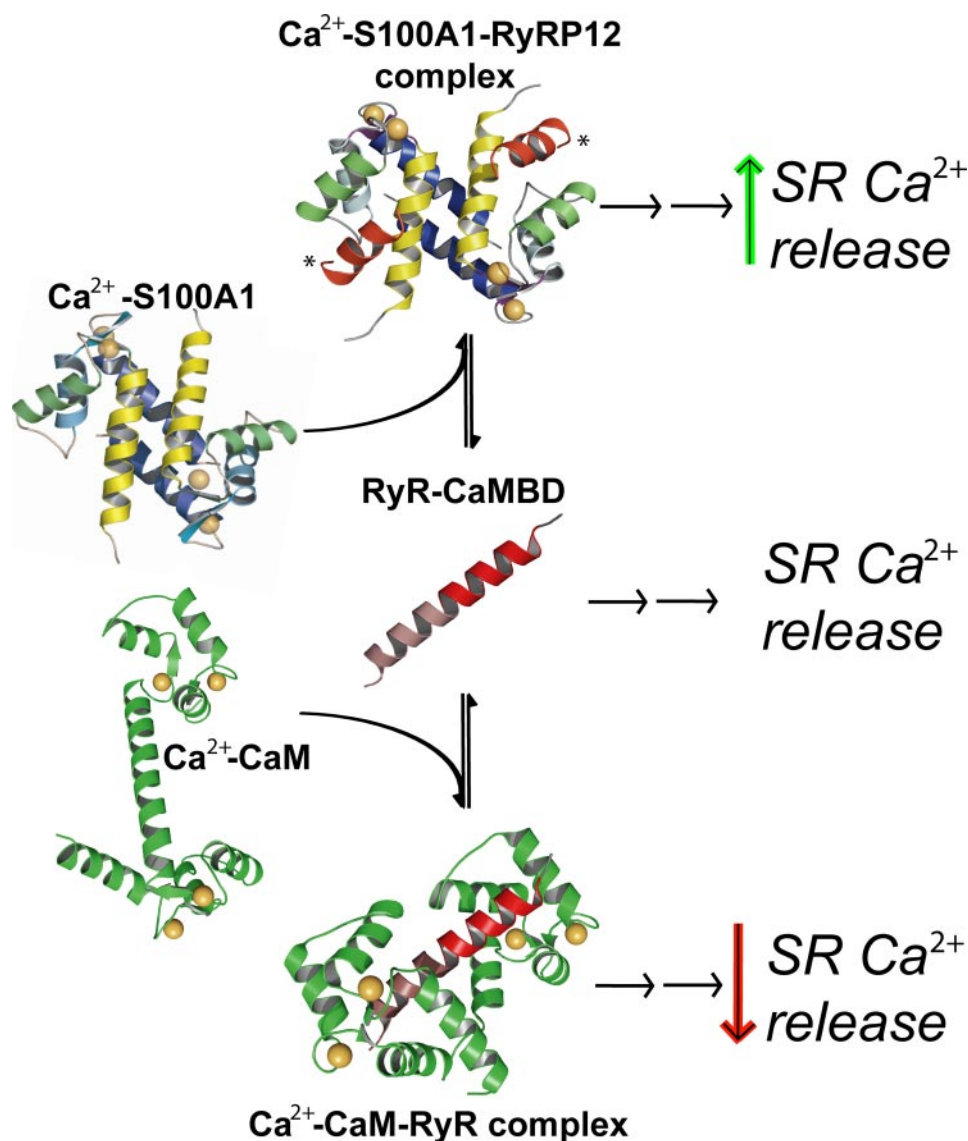
FIGURE 5. **Schematic of S100A1 function in skeletal muscle.** Ca^{2+}-S100A1 and Ca^{2+}-CaM bind to an overlapping region of RyR1 (*red*) in a Ca^{2+}-dependent manner. S100A1 binding leads to events that enhance SR calcium release. In contrast, calmodulin binding to this CaM binding domain leads to events that reduce SR calcium release. Competition between these two calcium-binding proteins for this target site may regulate SR Ca^{2+} release in skeletal muscle. The *asterisk* close to the Ca^{2+}-S100A1-RyRP12 structure denotes the location of the residues of RyR that are C-terminal to RyRP12 (residues 3616 –3627 of RyR) present in the longer RyR peptide (residues 3614 –3643 of RyR), used for structural studies when bound to CaM.

3620 and Leu-3624 are both almost completely buried at the S100A1-RyRP12 interface (Fig. 4*C*), and so it is not surprising that mutation of either of these hydrophobic residues abrogates the S100A1-RyRP12 interaction (6).

Although Ca^{2+}-S100A1 and Ca^{2+}-CaM both interact with an overlapping region of the RyR1 in a remarkably similar fashion, there are also several differences in the structures. The largest difference is that Ca^{2+}-CaM binds to a region of the RyR1 that extends 16 residues further toward the C terminus than the RyRP12 peptide. The continuation of the CaM-RyR interface gives this complex a substantially larger area of interaction than that of the RyRP12-S100A1 complex. Despite this larger area of binding, S100A1 and CaM each bind full-length RyR at comparable affinities at mid-nanomolar affinity (5, 27), and both S100A1 and CaM are able to compete intact RyR away from each other at comparable concentrations (Fig. 1*B*) (6).

One interesting feature of the S100A1-RyRP12 structure is its symmetry; the RyRP12 peptide binds with the same orientation to each S100A1 subunit, maintaining the symmetry present in S100 homodimers. This differs from the CaM-CaMBD structure, where only one peptide from RyR is present. The CaMBD is involved in intersubunit interactions and thus close in space to distal regions of the RyR (28). It is therefore tempting to speculate that the second subunit of S100A1 is involved in linking together two subunits of the RyR tetramer, whereas the primary S100A1-binding site in RyR is in the CaMBD, other secondary S100A1 binding regions have been suggested, and these sites also bind CaM weakly (5). Such a binding event may explain the discrepancy of affinity between the RyRP12 peptide and the intact RyR complex.

Based on these data, we present a model (Fig. 5) in which at physiologically elevated levels of calcium both Ca^{2+}-CaM and Ca^{2+}-S100A1 compete for the same binding site on RyR1. At elevated [Ca^{2+}], CaM is a strong inhibitor of RyR1, as evidenced by $^{45}Ca^{2+}$ release studies and [^3H]ryanodine binding studies (19). This led to the model that in the resting cell exogenous CaM induced some initial RyR activation, but as [Ca^{2+}] rises during the calcium transient, CaM inhibits RyR1 activity (19). In support of this model, recent experiments showed that the

bound to RyRP12 (residues 3616 –3627) and Ca^{2+}-CaM bound to a 30-residue peptide from an overlapping region of the RyR1 (residues 3614 –3643) (17) were compared. First, both RyR1 peptides were found to adopt a helical secondary structure when bound to Ca^{2+}-S100A1 and Ca^{2+}-CaM, respectively. In addition, important side chain interactions with Trp-3620 and three basic residues of RyR1 (Lys-3616, Lys-3622, and Lys-3626) were observed for both the S100A1- and CaM-peptide complexes (Fig. 4, *A*, *B* and *D*). In both complexes, Trp-3620 is central in anchoring the RyR peptide into the hydrophobic pocket of the protein. In contrast to what was observed here in the S100A1-RyRP12 peptide complex, Leu-3624 is only peripherally associated with the calmodulin hydrophobic pocket (17). Nonetheless, mutagenesis of either Leu-3624 (L3624D) or Trp-3620 (W3620A) of RyR1 was found to disrupt CaM binding to the intact RyR channel (15). For S100A1, Trp-

addition of recombinant CaM to skinned muscle fibers increased the frequency of Ca^{2+} sparks (29), but it also decreased the mass of Ca^{2+} release during a spark by roughly 37% (30). At elevated calcium levels, the ability of S100A1 to compete with a RyR1 antagonist such as Ca^{2+}-CaM is one possible explanation for how this S100 protein activates the RyR calcium release channel.

Recently, Rodney demonstrated that although exogenous CaM acts as a bimodal modulator of RyR1, endogenous CaM does not modulate RyR1-dependent Ca^{2+} release in skeletal muscle cells (30). Additionally, this study showed that endogenous CaM mostly localizes to the Z-line of skeletal muscle cells rather than the triad junction as found for S100A1 and RyR1. These data, taken with S100A1 data presented here and elsewhere (6, 8, 11), suggest that endogenous S100A1, but not endogenous CaM, directly modulates RyR activity. This alternative model could explain why exogenous CaM acts as an antagonist to RyR function. In this model, exogenous CaM overwhelms the endogenous RyR1 agonist S100A1, which in turn leads to decreased SR Ca^{2+} release. In both models presented (Fig. 5), the relative concentration of S100A1 to CaM at the triad junction is likely an important determinant for modulation of SR calcium release. How various protein concentrations regulate this critical region of the muscle fiber, and whether future studies can take advantage of this "turn up/turn down" switch of Ca^{2+} release to combat skeletal and cardiac myopathies is currently unknown and worthy of further investigation.

CONCLUSION

We have shown that Ca^{2+}-S100A1 specifically interacts with a discrete region of RyR, conserved between RyR1 and RyR2 isoforms. The solution structure of Ca^{2+}-S100A1 bound to a peptide from this region (RyRP12) reveals several hydrophobic and ionic interactions at the protein-peptide interface and is quite similar to a structure of this same region of the RyR bound to Ca^{2+}-CaM. This RyR-S100A1 interaction was also shown to increase SR Ca^{2+} release from the SR following electrical stimulation, and could have therapeutic implications for treatment of skeletal and cardiac myopathies. Likewise, it is important that small molecule inhibitors (*i.e.* drugs) designed to inhibit various enzymes and/or other protein targets do not inactivate S100A1, because this could trigger problems with heart and skeletal muscle.

REFERENCES

1. Fill, M., and Copello, J. A. (2002) *Physiol. Rev.* **82,** 893–922
2. Meissner, G. (1994) *Annu. Rev. Physiol.* **56,** 485–508
3. Westerblad, H., and Allen, D. G. (1991) *J. Gen. Physiol.* **98,** 615–635
4. Moore, C. P., Rodney, G., Zhang, J. Z., Santacruz-Toloza, L., Strasburg, G., and Hamilton, S. L. (1999) *Biochemistry* **38,** 8532–8537
5. Treves, S., Scutari, E., Robert, M., Groh, S., Ottolia, M., Prestipino, G., Ronjat, M., and Zorzato, F. (1997) *Biochemistry* **36,** 11496–11503
6. Prosser, B. L., Wright, N. T., Hernandez-Ochoa, E., Varney, K. M., Liu, Y., Olojo, R. O., Zimmer, D. B., Weber, D. J., and Schneider, M. F. (2008) *J. Biol. Chem.* **283,** 5046–5057
7. O'Driscoll, S., McCarthy, T. V., Eichinger, H. M., Erhardt, W., Lehmann-Horn, F., and Herrmann-Frank, A. (1996) *Biochem. J.* **319,** 421–426
8. Most, P., Remppis, A., Pleger, S. T., Loffler, E., Ehlermann, P., Bernotat, J., Kleuss, C., Heierhorst, J., Ruiz, P., Witt, H., Karczewski, P., Mao, L., Rockman, H. A., Duncan, S. J., Katus, H. A., and Koch, W. J. (2003) *J. Biol. Chem.* **278,** 33809–33817
9. Du, S. J., Cole, J. J., Tenis, N., Gao, X. M., Kontgen, F., Kemp, B. E., and Heierhorst, J. (2002) *Mol. Cell. Biol.* **22,** 2821–2829
10. Most, P., Remppis, A., Weber, C., Bernotat, J., Ehlermann, P., Pleger, S. T., Kirsch, W., Weber, M., Uttenweiler, D., Smith, G. L., Katus, H. A., and Fink, R. H. (2003) *J. Biol. Chem.* **278,** 26356–26364
11. Most, P., Pleger, S. T., Volkers, M., Heidt, B., Boerries, M., Weichenhan, D., Loffler, E., Janssen, P. M., Eckhart, A. D., Martini, J., Williams, M. L., Katus, H. A., Remppis, A., and Koch, W. J. (2004) *J. Clin. Investig.* **114,** 1550–1563
12. Wright, N. T., Varney, K. M., Ellis, K. C., Markowitz, J., Gitti, R. K., Zimmer, D. B., and Weber, D. J. (2005) *J. Mol. Biol.* **353,** 410–426
13. Rustandi, R. R., Baldisseri, D. M., Inman, K. G., Nizner, P., Hamilton, S. M., Landar, A., Landar, A., Zimmer, D. B., and Weber, D. J. (2002) *Biochemistry* **41,** 788–796
14. Donato, R. (2001) *Int. J. Biochem. Cell Biol.* **33,** 637–668
15. Yamaguchi, N., Xin, C., and Meissner, G. (2001) *J. Biol. Chem.* **276,** 22579–22585
16. Yamaguchi, N., Xu, L., Pasek, D. A., Evans, K. E., and Meissner, G. (2003) *J. Biol. Chem.* **278,** 23480–23486
17. Maximciuc, A. A., Putkey, J. A., Shamoo, Y., and Mackenzie, K. R. (2006) *Structure (Lond.)* **14,** 1547–1556
18. Samsó, M., and Wagenknecht, T. (2002) *J. Biol. Chem.* **277,** 1349–1353
19. Tripathy, A., Xu, L., Mann, G., and Meissner, G. (1995) *Biophys. J.* **69,** 106–119
20. Lipsitz, R. S., and Tjandra, N. (2004) *Annu. Rev. Biophys. Biomol. Struct.* **33,** 387–413
21. Inman, K. G., Yang, R., Rustandi, R. R., Miller, K. E., Baldisseri, D. M., and Weber, D. J. (2002) *J. Mol. Biol.* **324,** 1003–1014
22. Rustandi, R. R., Baldisseri, D. M., and Weber, D. J. (2000) *Nat. Struct. Biol.* **7,** 570–574
23. McClintock, K. A., and Shaw, G. S. (2003) *J. Biol. Chem.* **278,** 6251–6257
24. Bhattacharya, S., Large, E., Heizmann, C. W., Hemmings, B., and Chazin, W. J. (2003) *Biochemistry* **42,** 14416–14426
25. Santamaria-Kisiel, L., Rintala-Dempsey, A. C., and Shaw, G. S. (2006) *Biochem. J.* **296,** 201–214
26. Zimmer, D. B., Wright Sadosky, P., and Weber, D. J. (2003) *Microsc. Res. Tech.* **60,** 552–559
27. Rodney, G. G., Moore, C. P., Williams, B. Y., Zhang, J. Z., Krol, J., Pedersen, S. E., and Hamilton, S. L. (2001) *J. Biol. Chem.* **276,** 2069–2074
28. Zhang, H., Zhang, J. Z., Danila, C. I., and Hamilton, S. L. (2003) *J. Biol. Chem.* **278,** 8348–8355
29. Rodney, G. G., and Schneider, M. F. (2003) *Biophys. J.* **85,** 921–932
30. Rodney, G. G. (2008) *Am. J. Physiol.* **294,** 1288–1297
31. Bax, A., Grzesiek, S., Gronenborn, A. M., and Clore, G. M. (1994) *J. Magn. Reson. A* **106,** 269–273
32. Vuister, G. W., Kim, S. J., Orosz, A., Marquardt, J., Wu, C., and Bax, A. (1994) *Nat. Struct. Biol.* **1,** 605–614
33. Drohat, A. C., Baldisseri, D. M., Rustandi, R. R., and Weber, D. J. (1998) *Biochemistry* **37,** 2729–2740
34. Drohat, A. C., Tjandra, N., Baldisseri, D. M., and Weber, D. J. (1999) *Protein Sci.* **8,** 800–809
35. Wishart, D. S., Sykes, B. D., and Richards, F. M. (1992) *Biochemistry* **31,** 1647–1651
36. Brünger, A. T. (1993) *X-PLOR,* Version 3.1, Yale University Press, New Haven, CT
37. Tjandra, N., Omichinski, J. G., Gronenborn, A. M., Clore, G. M., and Bax, A. (1997) *Nat. Struct. Biol.* **4,** 732–738
38. Ottiger, M., Delaglio, F., and Bax, A. (1998) *J. Magn. Reson.* **131,** 373–378